Journal of Fluids and Structures (1999) **13,** 1069–1095
Article No.: jfls.1999.0242, available online at http://www.idealibrary.com on IDEAL®

PROPER ORTHOGONAL DECOMPOSITION OF RANDOM WIND PRESSURE FIELD

Y. TAMURA AND S. SUGANUMA

Department of Architecture, Tokyo Institute of Polytechnics, Atsugi, Kanagawa, Japan

H. KIKUCHI AND K. HIBI

Institute of Technology, Shimizu Corporation, Koto, Tokyo, Japan

(Received 19 October 1998 and in revised form 12 April 1999)

This paper discusses the application of the Proper Orthogonal Decomposition (POD) technique to randomly fluctuating wind pressure fields acting on a building surface. POD is a method of detecting a new coordinate system which can most efficiently represent the original fluctuating phenomena. This method can identify the deterministic or systematic structure hidden in the random fluctuations and thus help us to understand the phenomena better. It also demonstrates that the coordinate system employed is the most efficient, and can greatly reduce the amount of data that needs to be stored to re-examine the phenomena. Precautions in its application to random fields with mean values and with a singular condition are also mentioned. Furthermore, this paper introduces an example of the method's application to the evaluation of properties and the prediction of responses to wind forces acting on high-rise buildings; the validity of the method is also verified.

1. INTRODUCTION

THE CHARACTERISTICS AND INFORMATION INVOLVED in random fluctuations of wind speeds or wind pressures have so far been generally studied and identified through their probabilistic and statistical parameters, such as their probability distribution, cross-correlation function, cross-spectral density, and so on.

Proper Orthogonal Decomposition (POD) is a method used to derive the most efficient coordinate system for observing individual phenomena, in the same way as the Principal Component Analysis method. It can be applied to the analysis of random phenomena. Several applications to wind engineering have been studied, e.g. by Armitt (1968), Lee (1975), Best & Holmes (1983) and Kareem & Cermak (1984), who have demonstrated its advantages. Following the above first stage application of the POD technique, Holmes and his colleagues in particular put a lot of effort into developing the method, and made some outstanding contributions to the wind engineering field. For example, Holmes (1990) reviewed studies of the analysis and synthesis of pressure fluctuations on bluff bodies in complex turbulent flows using the POD technique, and Holmes (1992) applied POD to determining effective static wind load distributions on a low-rise building. Holmes *et al.* (1997) applied the POD technique to practical wind-resistant design of large roofs. However, because it was difficult to simultaneously measure the fluctuating wind speed and wind pressure at hundreds of points, the merits of POD application have not been sufficiently emphasized. Recently, there have been advances in instrumentation technology due to the development of computer systems. The multi-channel simultaneous fluctuating pressure measurement system developed by Fujii *et al.* (1986) and Ueda *et al.* (1994) can simultaneously

0889–9746/99/101069 + 27 $30.00

measure temporal data at 512 locations. This has greatly improved the quality of the tests themselves and increased the volume of data gathered. To fully utilize the merits of POD, the author and others have applied it and demonstrated its effectiveness. Bienkiewicz *et al.* (1995) and Tamura *et al.* (1995) have applied POD to fluctuating wind pressure fields on low-rise building models. Kikuchi *et al.* (1997) have applied it to fluctuating wind pressure fields on high-rise building models, taking measurements at up to 500 points by using a multi-channel simultaneous fluctuating pressure measurement system. They have shown that POD analysis can identify the systematic structure hidden in random fluctuations and thus greatly reduce the required amount of data that needs to be stored, by utilizing this efficient coordinate transformation.

This paper outlines the method and describes its characteristics, and demonstrates its effectiveness by an example application to fluctuating wind pressure fields. It also discusses points to note in the application of POD to random fields. Precautions in application to random fields with mean values and with a singular condition are mentioned. It is stressed that this method can be a very effective tool not only in wind engineering, but also in the analysis of random fields and system responses.

2. POD ANALYSIS OF RANDOM FIELD AND ITS MEANING

2.1. Pod Analysis

POD is a kind of Karhunen–Loève decomposition, which is a probabilistic expression of a method called Factor Analysis. This section briefly explains POD analysis based on Armitt (1968) and Bienkiewicz & Ham (1993) using a random fluctuating wind pressure field. The physical meaning is emphasized, although the mathematical expressions used may not precisely express some parts of the model.

It is assumed that the fluctuating wind pressure $p(x, y, t)$ is in the two-dimensional plane. Now, $p(x, y, t)$ is in principle only a fluctuating component with *a zero mean*. The purpose of the analysis is to find the deterministic coordinate function $\Phi(x, y)$ which best correlates with all the elements of a set of randomly fluctuating wind pressure fields. $\Phi(x, y)$ is derived to maximize the projection from the randomly fluctuating wind pressure field $p(x, y, t)$ to the deterministic function $\Phi(x, y)$, i.e., in order to realize from the probabilistic standpoint:

$$\iint p(x, y, t)\Phi(x, y)\,\mathrm{d}x\,\mathrm{d}y = \max. \tag{1}$$

By normalizing equation (1),

$$\frac{\iint p(x, y, t)\Phi(x, y)\,\mathrm{d}x\,\mathrm{d}y}{(\iint \Phi^2(x, y)\,\mathrm{d}x\,\mathrm{d}y)^{1/2}} = \max \tag{2}$$

is obtained. Since $p(x, y, t)$ can take positive and negative values, the above equation is maximized by a mean square method,

$$\frac{\overline{\iint p(x, y, t)\Phi(x, y)\,\mathrm{d}x\,\mathrm{d}y \iint p(x', y', t)\Phi(x', y')\,\mathrm{d}x'\,\mathrm{d}y'}}{\iint \Phi^2(x, y)\,\mathrm{d}x\,\mathrm{d}y} = \max, \tag{3}$$

where the bar of the numerator denotes the temporal average. This becomes an eigenvalue problem, and can be written as

$$\iint R_p(x, y, x', y')\Phi(x', y')\,\mathrm{d}x'\,\mathrm{d}y' = \lambda\Phi(x, y), \tag{4}$$

where $R_p(x, y, x', y')$ is a spatial correlation of the fluctuating wind pressure field. Where the fluctuating wind pressure is discretely given at M points uniformly distributed, it can be rewritten in the matrix form

$$\mathbf{R}_p\mathbf{\Phi} = \lambda\mathbf{\Phi}, \tag{5}$$

where $\mathbf{R}_p$ is a spatial correlation matrix of the fluctuating wind pressure and $M \times M$ square matrix. $\mathbf{\Phi}$ and λ denote an eigenvector and an eigenvalue of the spatial correlation matrix $\mathbf{R}_p$, respectively. The desired deterministic coordinate function is obtained as the eigenvector by solving equation (5). Since an $M \times M$ square matrix has, in principle, M eigenvectors $\mathbf{\Phi}_m$ $(m = 1, 2, \ldots, M)$, M deterministic coordinate functions are found. The mth eigenvector $\mathbf{\Phi}_m$ in the matrix form corresponds to the coordinate function $\Phi_m(x, y)$ in the functional form. By utilizing the orthogonality of the eigenvectors, the original fluctuating wind pressure field is expressed as

$$p(x, y, t) = \sum_{m=1}^{M} a_m(t)\Phi_m(x, y), \tag{6}$$

where, $a_m(t)$ is the mth principal coordinate given by

$$a_m(t) = \frac{\iint p(x, y, t)\Phi_m(x, y)\,\mathrm{d}x\,\mathrm{d}y}{\iint \Phi_m^2(x, y)\,\mathrm{d}x\,\mathrm{d}y}. \tag{7}$$

The mth eigenvector $\Phi_m(x, y)$ is called the mth eigenmode. It is noted that, as implied by equation (6) using the expression with Σ, the integral of equation (7) has the meaning of simple spatial total sum. For simplicity, the eigenvectors are normalized by letting the denominator of equation (7) be unity as described in the following:

$$\iint \Phi_m^2(x, y)\,\mathrm{d}x\,\mathrm{d}y = 1. \tag{8}$$

The lower eigenmode can bring out in full relief the systematic structure hidden in the random fluctuating wind pressure field, as discussed later. Therefore, it might be possible to find a physical meaning that corresponds to the lower-order principal coordinate. Let δ_{mn} be Kronecker's delta. The mean product of the mth and nth principal coordinates is expressed as

$$\overline{a_m(t)a_n(t)} = \lambda_m\delta_{mn}. \tag{9}$$

This equation shows that the correlation between two principal coordinates having differing orders, $a_m(t)$ and $a_n(t)$ $(m \neq n)$ is zero, i.e., they are uncorrelated and the eigenvalue λ_m is equal to the mean square of the mth principal coordinates:

$$\overline{a_m^2(t)} = \lambda_m. \tag{10}$$

Furthermore, the mean square of wind pressure at a point (x, y) is expressed as

$$\overline{p^2(x, y, t)} = \sum_{m=1}^{M} \lambda_m\Phi_m^2(x, y). \tag{11}$$

It is noted that the field-total sum of the mean-square field of the fluctuating wind pressure is equal to the sum of the eigenvalues. Thus, it is equal to the sum of the mean squares of the principal coordinates:

$$\iint \overline{p^2(x, y, t)}\,\mathrm{d}x\,\mathrm{d}y = \iint \left\{ \sum_{m=1}^{M} \lambda_m\Phi_m^2(x, y) \right\} \mathrm{d}x\,\mathrm{d}y = \sum_{m=1}^{M} \lambda_m = \sum_{m=1}^{M} \overline{a_m^2(t)}. \tag{12}$$

Meanwhile, POD analysis has to be conducted in principle on the fluctuating components after subtracting the mean components, as discussed later. If the mean value is included, the original meaning of the principal coordinate is distorted, and attention needs to be paid to this phenomenon. That is, $\mathbf{R}_p$ in equation (5) is actually a covariance matrix. Furthermore, equation (12) implies that the field-total sum of the variance of fluctuating wind pressures is equal to the sum of the eigenvalues and it is equal to the sum of the variance of the principal coordinates, as seen in equation (10). It follows that the sum of the diagonal elements of matrix $\mathbf{R}_p$ becomes the sum of the eigenvalues.

When simultaneously dealing with the fluctuating wind pressure field and the fluctuating wind speed field or considering the correlation of variables in differing unit systems, homogenization of the variables is necessary. In this case, the variables standardized with the standard deviation of unity at the mean value of zero are often employed, where $\mathbf{R}_p$ becomes the correlation coefficient matrix. Indeed, the meanings of the eigenvalue, eigenvector and principal coordinate change in individual cases.

When the eigenmode $\Phi_m(x, y)$ and the principal coordinate $a_m(t)$ are obtained in the above way, to be rigorous, the original fluctuating wind pressure field is expressed by equation (6). However, reconstruction in the lower modes up to the Nth, where $N < M$, is often accurate enough in an engineering sense and it can be approximated by

$$\hat{p}(x, y, t) = \sum_{m=1}^{N} a_m(t)\Phi_m(x, y) \quad (N < M). \tag{13}$$

The number of modes appropriate to the reconstruction can be estimated by the proportion c_m and the cumulative proportion C_N, defined next. The proportion of the mth principal coordinate is defined as

$$c_m = \frac{\lambda_m}{\sum_{m=1}^{M} \lambda_m}. \tag{14}$$

Furthermore, this denotes the ratio of the mth eigenvalue to the sum of the eigenvalues, or the ratio of the variance of the mth principal coordinate to the field-total sum of the variance. The cumulative proportion up to the Nth mode is defined as

$$C_N = \sum_{m=1}^{N} c_m. \tag{15}$$

The error level of the fluctuating wind pressure reconstructed according to equation (13) using up to the Nth mode is estimated from $1 - C_N$.

2.2. Meaning of Pod Analysis

Since POD has already been used in wind engineering, it seems unnecessary to explain it in plain terms here. However, since many researchers do not use it appropriately, e.g. in connection with inclusion of mean components, it would be instructive to briefly explain the meaning of POD by using simple samples of fluctuating wind pressures $p_1(t)$, $p_2(t)$ and $p_3(t)$ measured at three points. For convenience of subsequent discussion on the mean value components, $p_1(t)$, $p_2(t)$ and $p_3(t)$ are assumed to contain the mean values in this section. Figure 1 shows the temporal variations of the three wind pressure signals. Generally, the periodicity hidden in such a random original fluctuation, the behavior of the advection of the disturbance, and so on are identified by observing Figure 1 with the help of information such as the cross-correlation function, cross-spectral density and so on.

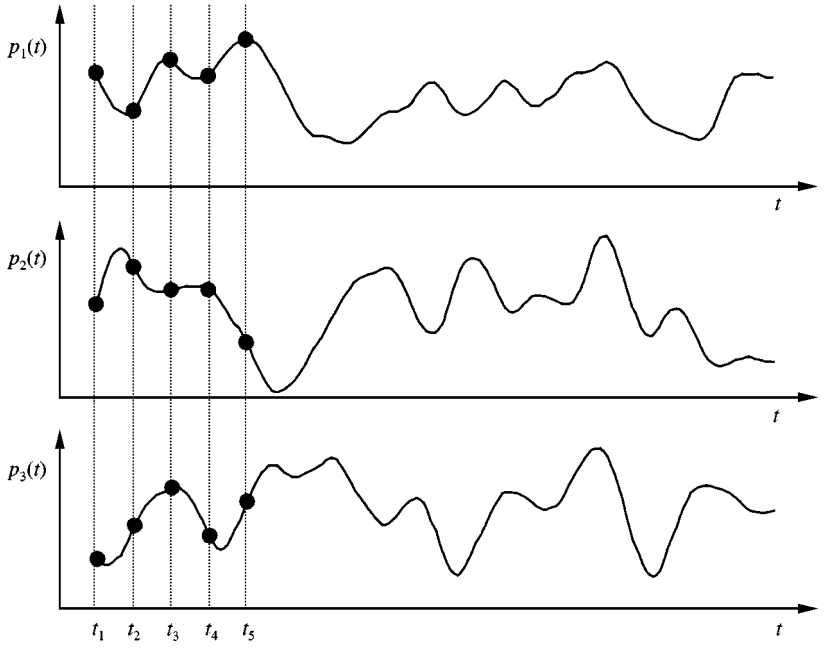

Figure 1. Fluctuating wind pressure.

By the way, this is not simply a method of graphically showing the time-history of the fluctuating wind pressure field. Tamura (1995) represented the instantaneous state of the wind pressure field by a point in space consisting of the mutually orthogonal $p_1(t)$, $p_2(t)$ and $p_3(t)$ axes. Thus, the record of the fluctuating pressure field for a given period can be expressed by a trace of the point movement in the three-dimensional pressure space, as shown in Figure 2. The trace of the movement is called "state locus" in Tamura (1995). Temporal variation of the wind pressure field is thus completely represented by the state locus. If there are more than three measuring points, graphical presentation becomes difficult, but this does not lose generality. The instantaneous wind pressure field composed of M pressure signals, i.e., $p_1(t)$, $p_2(t)$, $\ldots$, $p_M(t)$, shall be expressed by a point in M-dimensional space, and even in such a situation, the temporal variation of the whole wind pressure field can be captured only by the state locus. Figure 2 is drawn with the original physical coordinates of the measured fluctuating wind pressures, but these coordinates are not always optimum for observing the field. The POD analysis searches for a new mutually orthogonal coordinate system which can most efficiently capture the state locus. The phenomena are observed by projecting the state locus onto this coordinate system, and this new coordinate system is the principal coordinate system expressed in equation (7).

If the state locus shown in Figure 2 exists on a single plane (π-plane), it is better to stop using the original three-dimensional physical coordinates and to observe the phenomena on the π-plane. Since all the information of the fluctuating wind pressure field is included on this plane, the state locus can be represented using only the two-dimensional orthogonal coordinates of $\xi(t)$ and $\eta(t)$ on the π-plane, thus achieving a significant reduction in complexity. Simplification of information not only helps us to understand the phenomena, but can also economize the amount of data that needs to be stored for the simulation. Even when employing the new orthogonal coordinate system on the π-plane, an infinite number of orthogonal coordinate systems can be chosen on this π-plane. Thus, by setting the

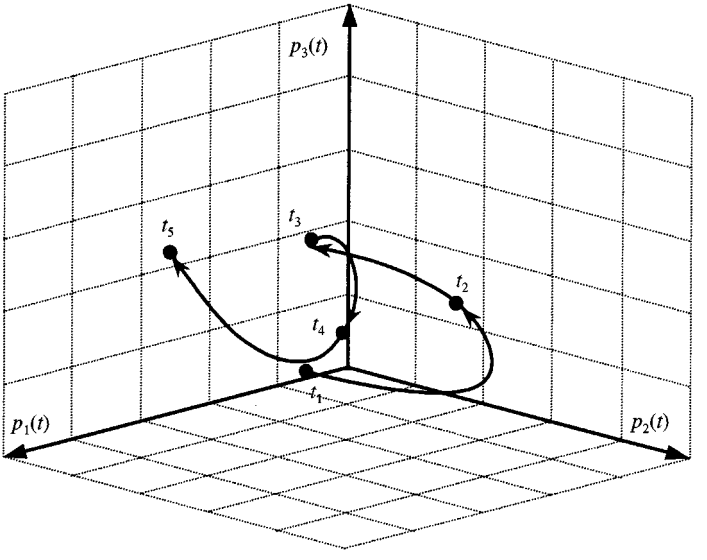

Figure 2. State locus of fluctuating wind pressure field.

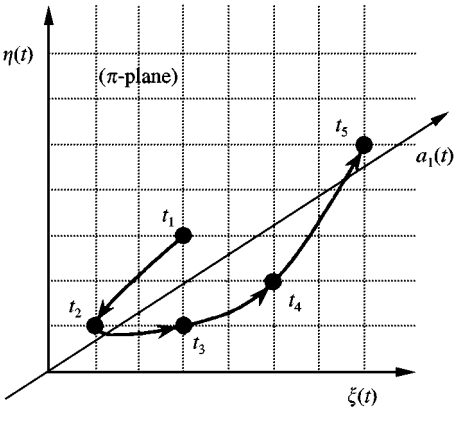

Figure 3. State locus on same plane.

temporary coordinate system of $\xi(t)$ and $\eta(t)$ on the π-plane as shown in Figure 3, the state locus of the fluctuating wind pressure is depicted on this coordinate system. Here, it is seen in this particular case that the state locus in Figure 3 tends to increase toward the right. Thus, by taking a new coordinate axis $a_1(t)$ in this direction, if the state locus is projected onto this axis, most of the information is also included on it. Therefore, the characteristics of the wind pressure fluctuation can be almost entirely represented by the variation of the value of the new coordinate $a_1(t)$. In the extreme case, provided that the state locus is just on a line as shown in Figure 4 and the coordinate $a_1(t)$ is made to match with this line, all wind pressure field information can be described only by the one-dimensional axis $a_1(t)$. Here, it is meaningless to observe the phenomenon by leaving the physical coordinates $p_1(t)$, $p_2(t)$ and $p_3(t)$ as they are. Although there are no such extreme cases, there is an axis which contains the largest amount of fluctuation information. This is the axis which has the largest projection from each point on the state locus.

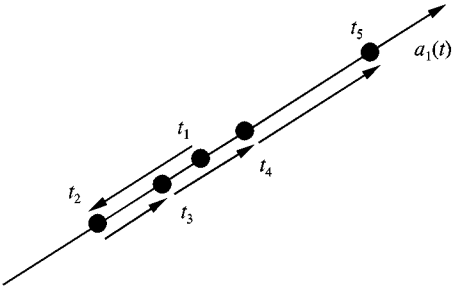

Figure 4. State locus on same line.

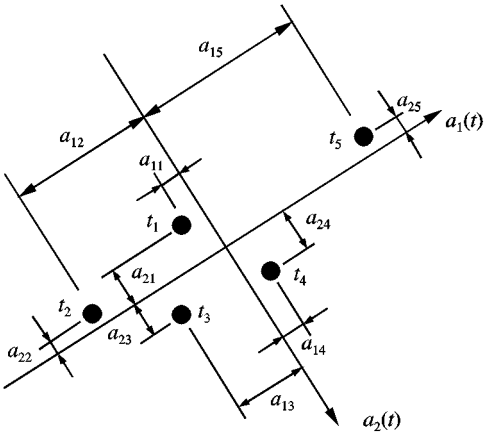

Figure 5. Projection of state locus onto principal coordinate.

The following procedure will make the projection to the coordinate axis largest. As shown in Figure 5, the origin of axis $a_1(t)$ is taken at the position of the average value of the state locus, thus maximizing the mean square of the readings a_{1j}, obtained by projecting each point onto the axis $a_1(t)$ as

$$\sigma_{n1}^2 = \frac{1}{M} \sum_{j=1}^{M} a_{1j}^2. \tag{16}$$

It is noted that since the origin of the axis $a_1(t)$ is set to the position of the mean state locus, equation (16) in fact expresses the variance. This is not the mean square of the pressure at all. This is an important point, and it is discussed in detail in the next section.

At any rate, the most efficient new coordinate $a_1(t)$ can represent the random field. The vector representing the direction of the coordinate axis is called the 1st eigenvector. Furthermore, the reading $a_1(t)$ obtained by projecting the state locus in the fluctuating wind pressure field to this new coordinate is called the first principal coordinate. The variance of equation (16) corresponds to the first eigenvalue. The information presented by the principal coordinate $a_1(t)$ in Figure 5 comprises only the projected readings a_{11} through a_{15}, but lacks information in the orthogonal direction. Since the state locus of the fluctuating wind pressure field also has components in the axis orthogonal to $a_1(t)$, the first principal coordinate cannot completely describe the fluctuating wind pressure. Thus, if the additional principal coordinate axis $a_2(t)$ orthogonal to the axis $a_1(t)$ is employed, the values

a_{21} through a_{25} projected from the state locus to the axis of $a_2(t)$ comprise the rest of the information, and the two axes $a_1(t)$ and $a_2(t)$ can completely describe the fluctuating wind pressure field in this particular case.

The principle is that the coordinate axis (the 1st mode) is first determined to maximize the variance. The coordinate axis (the 2nd mode) orthogonal to this is next determined to maximize the variance in the coordinate axis. Further, the coordinate axis (the 3rd mode) orthogonal to these axes is determined to maximize the variance in the coordinate axis. If there are a total of M fluctuating wind pressures, M coordinate axes are obtained by repeating this process. However, in the real analysis, after solving the eigenvalue problem of equation (5), M eigenvectors and principal coordinates are mathematically determined.

2.3. Distortion by Mean Value Components

2.3.1. *Comparison of the eigenvectors of a pressure field with/without mean value components*

Figures 6 and 7 compare the lowest three modes of the pressure field on a low-rise building model obtained by two different ways of calculating the spatial correlation matrix: with and without inclusion of the mean value components. Here, the fluctuating wind pressures were measured simultaneously at 494 pressure taps on the roof and the four wall surfaces of the model by using a multi-channel simultaneous fluctuating pressure measurement system (Ueda *et al.* 1994). However, the POD analysis was repeated for pressures on each of the building surfaces treated separately. As shown in Tamura *et al.* (1995), the eigenvalues and eigenvectors of the entire pressure field on the model consisted of all 494 pressure taps, and those of the pressure field on each of the model surfaces are different.

Table 1 compares the eigenvalues and proportions for the roof pressure field consisting of 204 pressure taps for the two cases. The distributions of the mean pressure coefficient and the fluctuating pressure coefficient (standard deviation) for this model are shown in Figures 8 and 9.

Even for the same original pressure field, the eigenvectors obtained are quite different, depending upon whether or not the spatial correlation matrix includes the mean value components. The proportions of the 1st modes are also quite different, as shown in Table 1: 98·0% with inclusion of the mean value, and 40·2% without inclusion. It is obvious that the mean value components provide quite different results and can lead to a different understanding of the phenomena. Therefore, the question of whether or not the mean value should be included has to be clarified.

In some wind engineering studies using the POD technique, e.g. Bienkiewicz & Ham (1993), Davenport (1995) and Santi & Hémon (1998), the mean value components were included in the calculation of the spatial correlation matrix. The authors' group had also included the mean value components in the early stage of its utilization of the POD technique, e.g. Bienkiewicz *et al.* (1995) and Tamura *et al.* (1995).

Incidentally, the POD technique is the method of finding the most efficient axis which has the most energy in terms of the mean square. As discussed in the previous section and as shown in Figure 3, the most expanded directions of the state locus are sought out sequentially. Thus, looking at the state locus, it is not difficult to understand that the mean value component should not be included in the calculation of the correlation matrix.

Here, it would be worthwhile to demonstrate the necessity of excluding the mean value in the POD analysis and the spatial correlation matrix is calculated over all surfaces. Note that the same discussion is available for different mode shapes obtained by using a subset of the full correlation matrix associated with each surface.

2.3.2. *Physical consideration of POD with/without inclusion of mean value components*

To keep matters simple, a two-variable random field, i.e., $p_1(t)$ and $p_2(t)$, is considered. Figure 10 shows an example of the state locus of the random field. The physical coordinate $(p_1(t), p_2(t))$ moves around the mean position (p_{1m}, p_{2m}), and the state locus is extended for a particular direction. It is obvious that this particular direction is the 1st principal coordinate, and the second principal coordinate shall be normal to the first mode direction.

Here, the principal coordinates were also derived in two ways: one where the mean value components were subtracted from the variables for the calculation of the space correlation matrix; and the other including the mean values.

Table 2 and Figure 10 compare the obtained eigenvalues and eigenvectors of the space correlation matrices by the above two different methods. With inclusion of the mean value components, the 1st mode and the 2nd mode eigenvalues are 103·1 and 2·03, which results in 98 and 2% proportions, respectively. This result is never consistent with Figure 10. In the figure, the ratio of the lengths of the two principal axes of the elliptic shape of the state locus is almost 2 : 1, which suggests that the ratio of the eigenvalues of the 1st mode and 2nd mode may be almost $2^2 : 1^2$. However, without inclusion of the mean value components, the eigenvalues of the 1st mode and 2nd mode are 4·11 and 1·02, and their contributions are 80 and 20%, respectively. This result can reasonably explain the state locus shown in Figure 10.

The eigenvectors are also depicted in Figure 10. Without inclusion of the mean-value components, as indicated by solid lines, the 1st mode eigenvector is directed almost along the longer axis of the elliptic state locus and the 2nd mode along the minor elliptic axis. On the other hand, with inclusion of the mean value components, as indicated by broken lines, the direction of the 1st mode eigenvector almost coincides with that of the mean value vector, and the 2nd mode eigenvector is simply normal to the 1st mode eigenvector. The 1st mode and 2nd mode eigenvectors are basically governed by the direction of the mean value vector, but do not have an essential relation with the characteristics of the fluctuating components represented by the elliptic state locus.

Generally, inclusion of the mean value components results in a significant 1st mode proportion, such as 98 or 99%, and the 1st mode eigenvector tends to be almost identical to the mean value vector as shown in Figure 10. The latter implies that the 1st mode shape with inclusion of the mean value components becomes almost similar to the mean value distribution. However, as seen from Figure 10, the actual fluctuation of the random field does not necessarily relate to the direction of the mean value vector. Thus, inclusion of the mean value vector distorts the true eigenvectors, and it is obvious that such eigenmodes cannot help us to understand the randomly fluctuating field. The parameter to be maximized in equation (16) should actually be the "variance", not the "mean square". The variable $p(x, y, t)$ used in the POD analysis should be derived as the fluctuating component by subtracting the mean value from the pressure data. It should be noted that, even if the spatial correlation matrix includes the mean values, its eigenvectors are of course mutually orthogonal, because they are derived as the mathematical eigenvalue solutions of any matrix. Furthermore, the fully reconstructed signals also coincide with the original ones. These are mathematically valid, but are unrelated to a physical validity. This fact could lead to misunderstanding of the POD technique, and to misuse of the correlation matrix with inclusion of the mean value components.

Here, the following fact would be important for the wind pressure field. If the direction of the true 1st mode eigenvector coincides with that of the mean value vector or the 1st mode shape and the distribution of mean values are similar, there might be no large difference between the spatial correlation matrices with and without inclusion of the mean value

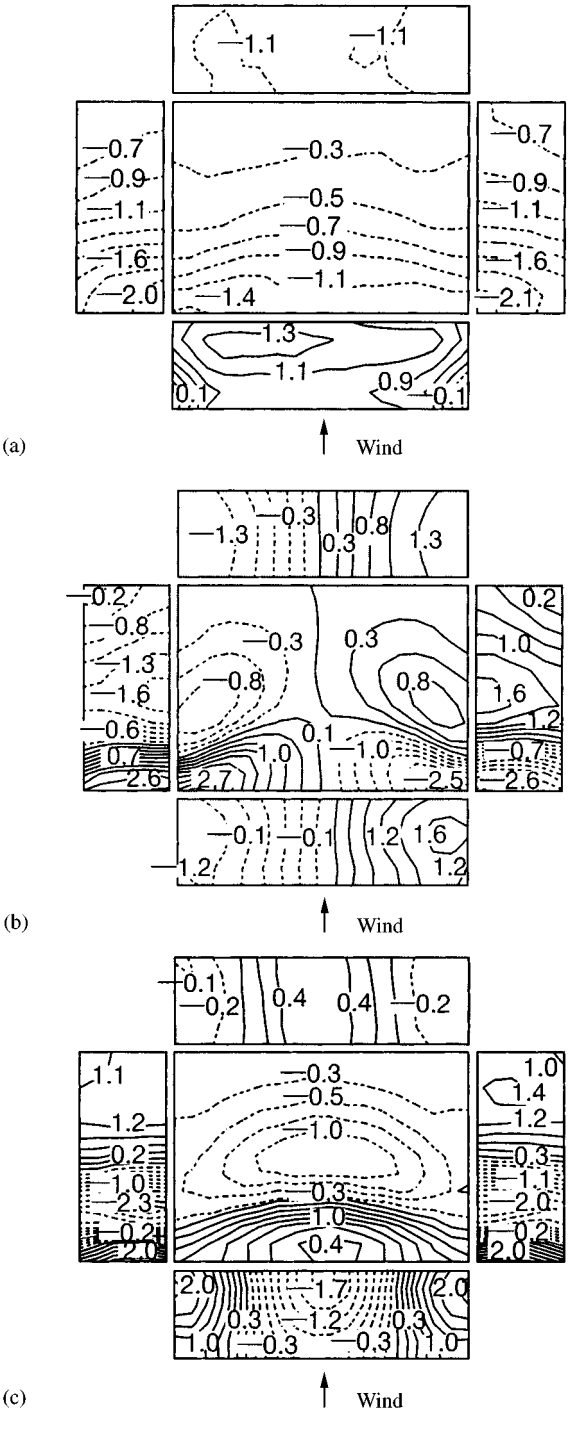

Figure 6. Eigenvectors for the lowest three modes of fluctuating pressures on surfaces of a low-rise building model with inclusion of mean value components: (a) 1st mode; (b) 2nd mode; (c) 3rd mode.

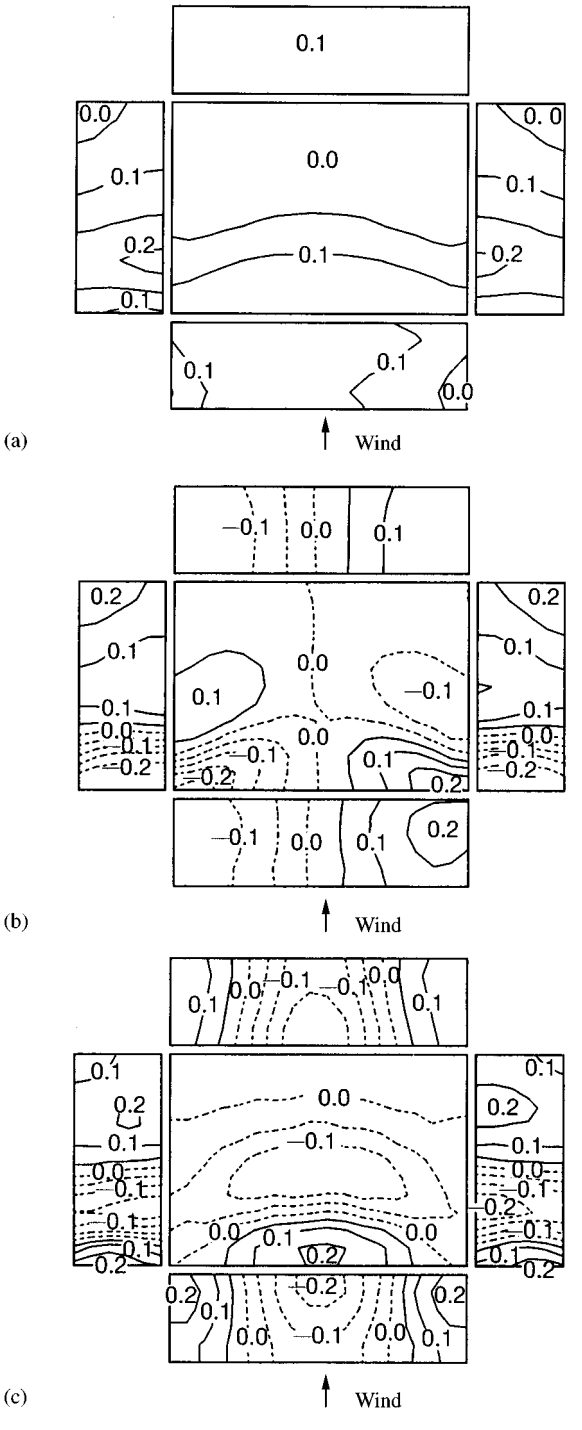

Figure 7. Eigenvectors for the lowest three modes of fluctuating pressures on surfaces of a low-rise building model without inclusion of mean value components: (a) 1st mode; (b) 2nd mode; (c) 3rd mode.

TABLE 1

Comparison of eigenvalues and proportions with/without inclusion of mean value components for the first 10 modes for roof pressures on a low-rise building model

	Without mean value		With mean value	
Mode	Eigenvalue	Proportion (%)	Eigenvalue	Proportion (%)
1st	1411	40·20	22 970	98·00
2nd	295	8·40	223	0·95
3rd	224	6·39	40	0·17
4th	175	4·98	28	0·12
5th	128	3·66	21	0·09
6th	102	2·91	14	0·06
7th	80	2·29	9	0·04
8th	75	2·12	8	0·03
9th	61	1·74	8	0·03
10th	53	1·51	6	0·02

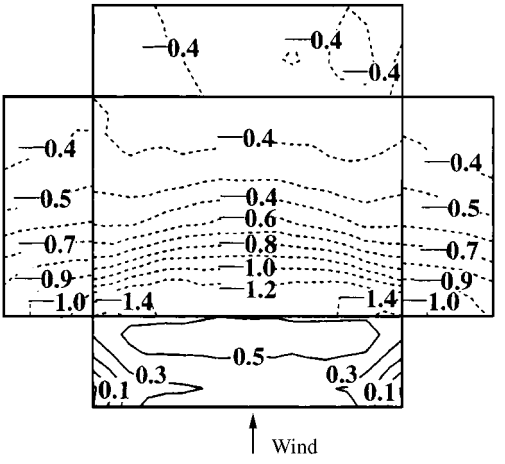

Figure 8. Distribution of mean pressure coefficients on surfaces of a low-rise building model.

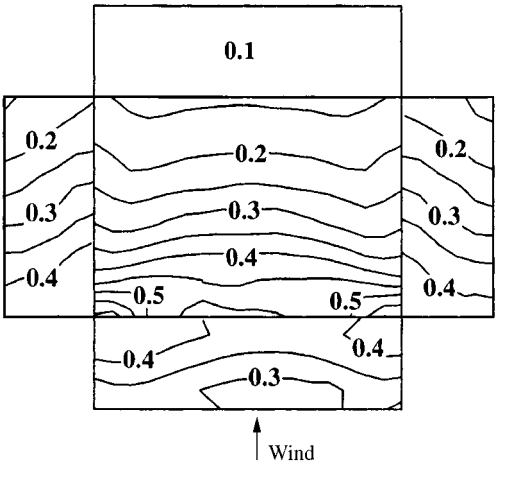

Figure 9. Distribution of fluctuating pressure coefficients (standard deviation) on surfaces of a low-rise building model.

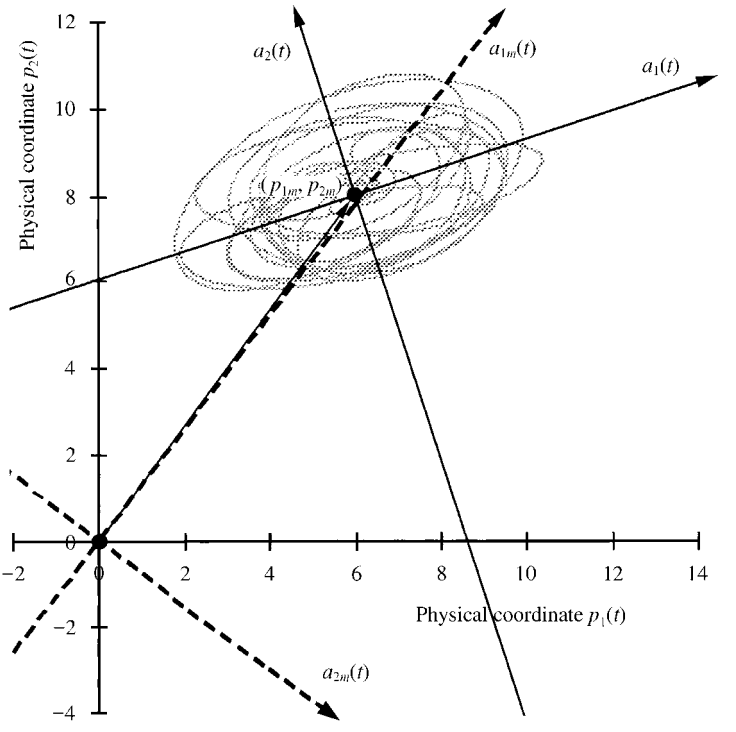

Figure 10. A state locus of a simple two-variable random field and eigenvectors obtained with (dotted lines) and without (solid lines) inclusion of mean value components.

TABLE 2

Comparison of eigenvalues and proportions with/without inclusion of mean value components for the random field shown in Figure 10

	Without mean value		With mean value	
Mode	Eigenvalue	Proportion (%)	Eigenvalue	Proportion (%)
1st	4·11	80·1	103·11	98·1
2nd	1·02	19·9	2·03	1·9

components. If the quasi-steady assumption is valid for the u-component, the pressure field fluctuates, keeping the spatial distribution proportional to the mean pressure distribution. Therefore, if the true 1st mode contribution predominates, its mode shape should be similar to the mean pressure distribution under the quasi-steady assumption. Thus, the direction of the true 1st mode eigenvector and the mean value vector can be one of the measures for examining the quasi-steady assumption of the pressure field. However, even if such a condition is expected, this cannot be a reason for including the mean value components in the POD analysis. The mean value should be excluded from the POD analysis, and its contribution could be examined separately.

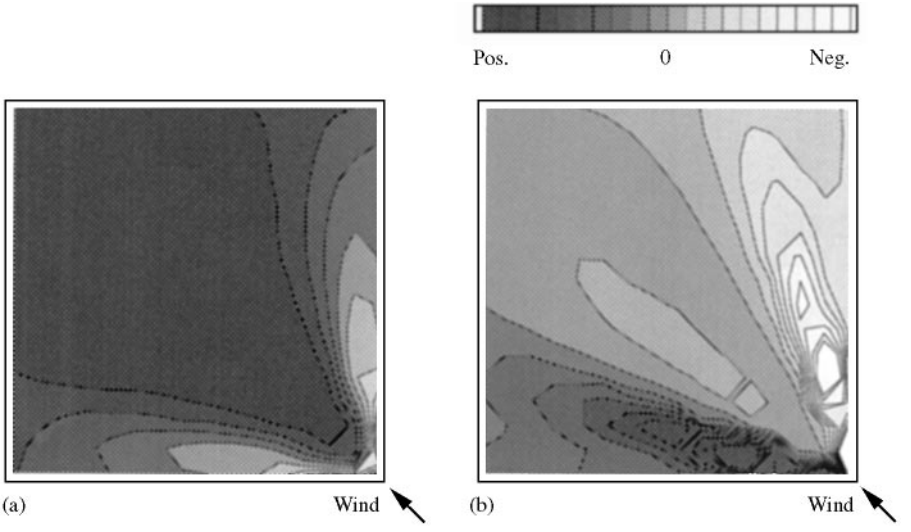

Figure 11. Eigenvectors (mode shapes) for sample A of the roof pressures obtained under the same wind conditions as sample B: (a) 1st mode; (b) 2nd mode.

TABLE 3
Proportions of the first six modes for two samples of the roof pressure field on a low-rise building model obtained under the same wind conditions

Mode	Sample A	Sample B
1st	29·2%	30·6%
2nd	25·4	24·7
3rd	7·0	6·3
4th	3·1	3·4
5th	2·8	2·7
6th	2·3	2·4

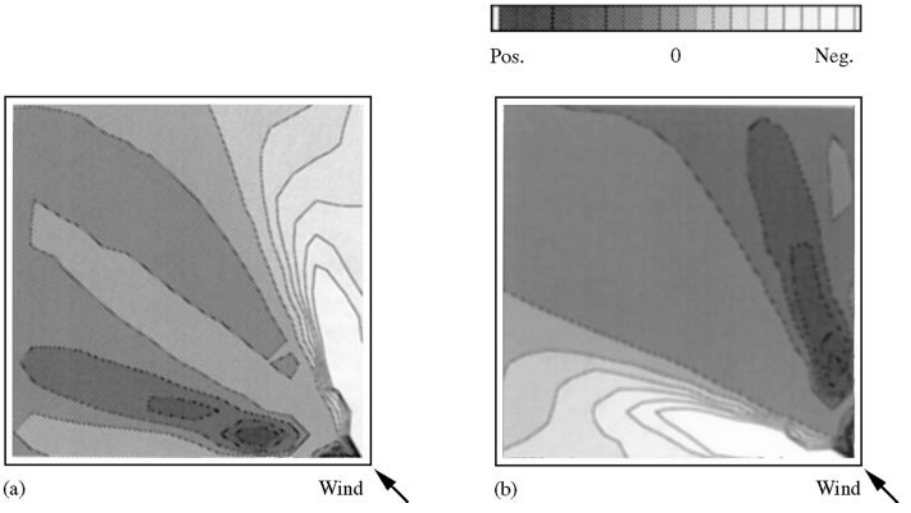

Figure 12. Eigenvectors (mode shapes) for sample B of the roof pressures obtained under the same wind conditions as sample A: (a) 1st mode; (b) 2nd mode.

2.4. POD OF RANDOM FIELD WITH A SINGULAR CONDITION

In this section, it is demonstrated that the POD analysis does not always find effective coordinates. Since it refers to an eigenvalue problem for the correlation (covariance) matrix $\mathbf{R}_p$, results are not as expected when the eigenvalues become multiple roots. For example, provided that there are two uncorrelated wind pressures with unit variances, the covariance matrix is a second-order identity matrix. Therefore, the eigenvalues become multiple roots and the eigenvectors cannot be uniquely determined in the sense of the POD analysis. Such extreme cases do not happen in reality and the apparent eigenvectors are obtained. This can further confuse the actual phenomena. However, if such characteristics of the POD are well understood, the phenomena can be inversely analyzed from these incidents.

A case was studied of fluctuating wind pressures on the square flat roof of a low-rise building in which the wind approached diagonally (45°). The fluctuating wind pressures were measured simultaneously at 256 pressure taps on the roof of the model, using the multi-channel simultaneous fluctuating pressure measurement system.

Figures 11 and 12 show the 1st mode eigenvector, i.e., mode shape, $\mathbf{\Phi}_1$ and the 2nd mode eigenvector $\mathbf{\Phi}_2$ obtained from two different samples under the same conditions. Here, it is the matter of course that both samples do not include mean value components. In sample A, as shown in Figure 11, $\mathbf{\Phi}_1$ and $\mathbf{\Phi}_2$ are symmetric and antisymmetric, respectively, with respect to the diagonal. In another sample B, as shown in Figure 12, both modes are asymmetric but $\mathbf{\Phi}_1$ and $\mathbf{\Phi}_2$ are symmetric with each other. Table 3 shows the proportions up to the 6th mode for samples A and B. In both of these samples, the 1st and the 2nd modes are dominant and their proportions are almost equal. This suggests the existence of a singular condition where two uncorrelated phenomena can contribute equally to the fluctuating wind pressure field. This singular condition could not be completely satisfied due to the uncertainties of the measured data. As a result, there was some difference in their proportions and contingent mode shapes were determined. However, it is considered that there was no structural difference between the two samples. Figure 13 shows the state locus for samples A and B projected on the first and second principal coordinate plane. The

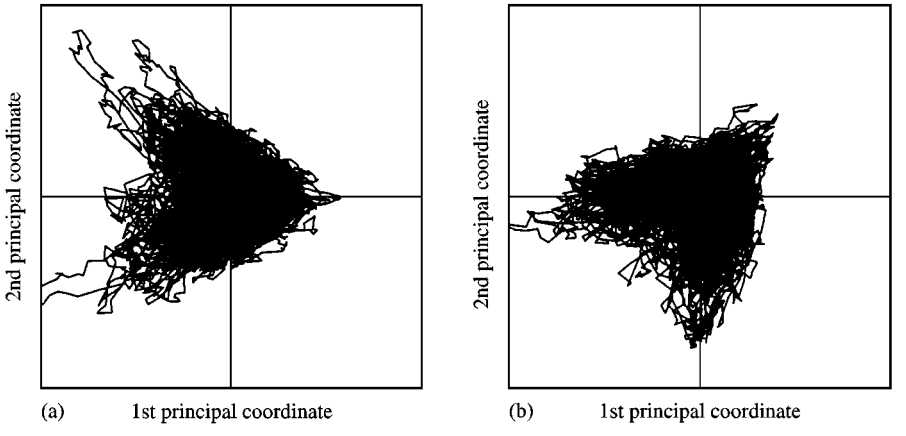

Figure 13. State loci for the two samples of the roof pressures obtained under the same wind conditions: (a) sample A; (b) sample B.

samples show almost the same wedge-shaped distribution, although their directions differ. This supports the above discussions.

Holmes *et al.* (1996) describes another important special case in which the covariance matrix is homogeneous. In this case, the eigenvectors form a Fourier series and the POD becomes equivalent to a spectral analysis.

3. POD ANALYSIS FOR WIND PRESSURE ACTING ON TALL BUILDINGS

As an example demonstrating the effectiveness of POD in analyzing pressure fields as well as responses, the application of POD to wind pressure fields on tall building models is presented in this section.

Wind tunnel experiments were conducted using the approaching wind with a length scale of $\frac{1}{400}$ for a suburban terrain where the power-law index of the mean wind speed profile was $\frac{1}{6}$. Figure 14 shows a tall building model which is 10 cm square and 50 cm high. It has 500 wind pressure taps uniformly distributed over the surface of its four walls. The wind pressure was measured simultaneously at all points using the multi-channel simultaneous fluctuating pressure measurement system. The wind direction was set normal to the wall face. The sampling interval of the fluctuating wind pressure was 0·00128 s, and 32 768 samples were obtained continuously for about 42 s. The reduced scale of time was about $\frac{1}{100}$ and the data length of the experiments was equivalent to an actual time of about 70 min. It is noted that the distortion of the pressure signals due to the connecting tube from the taps to the sensors was corrected on the basis of the pre-obtained gain and phase characteristics.

3.1. Distribution of Wind Pressure Coefficient

Figures 15 and 16 show the mean and the fluctuating wind pressure coefficients. They are the temporal mean and the standard deviation of the wind pressure at each point, respectively, normalized by the mean velocity pressure at building roof height H. The positive pressure on the windward wall increased at heights around $0{\cdot}75H$–$0{\cdot}8H$ and decreased at the peripheral and the lower portions, as shown in Figure 15. The negative pressures on the side and leeward walls were distributed relatively uniformly and did not

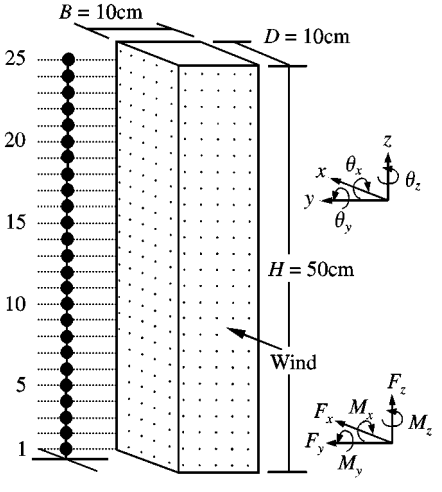

Figure 14. Pressure measurement model and analytical lumped-mass model for a high-rise building.

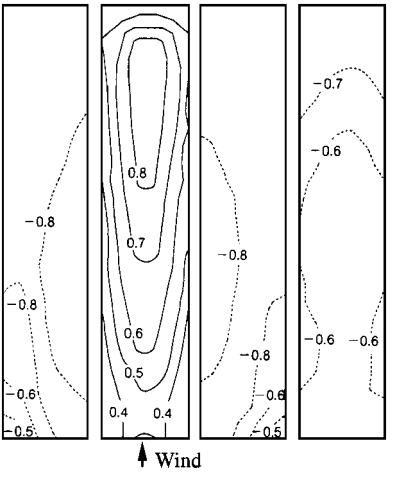

Figure 15. Distribution of mean wind pressure coefficient on a high-rise building model.

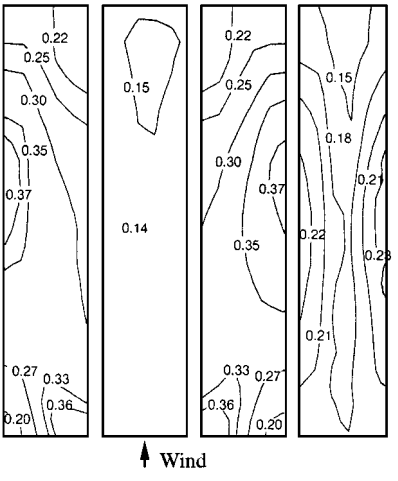

Figure 16. Distribution of fluctuating wind pressure coefficient on a high-rise building model.

change much vertically. The fluctuating wind pressures shown in Figure 16 were distributed fairly uniformly on the windward wall, but changed in a slightly complicated manner on the side and windward walls. These changes indicate the effects of the vortices shed from the side to the wake of the building and the flow patterns with irregular and three-dimensional disturbance caused by the flow separation from the windward edges of the building.

3.2. Mode Shape

The subject to be analyzed was a 500×500 matrix whose diagonal and nondiagonal elements were the variance and the covariance of fluctuating wind pressures, respectively. It had 500 eigenvalues and eigenvectors. Figure 17(a–e) shows the lowest five eigenvectors (mode shapes).

The 1st mode shape is bilaterally antisymmetric, as shown in Figure 17(a). As described later, the 1st mode is closely related to the vortex shedding and becomes dominant for the

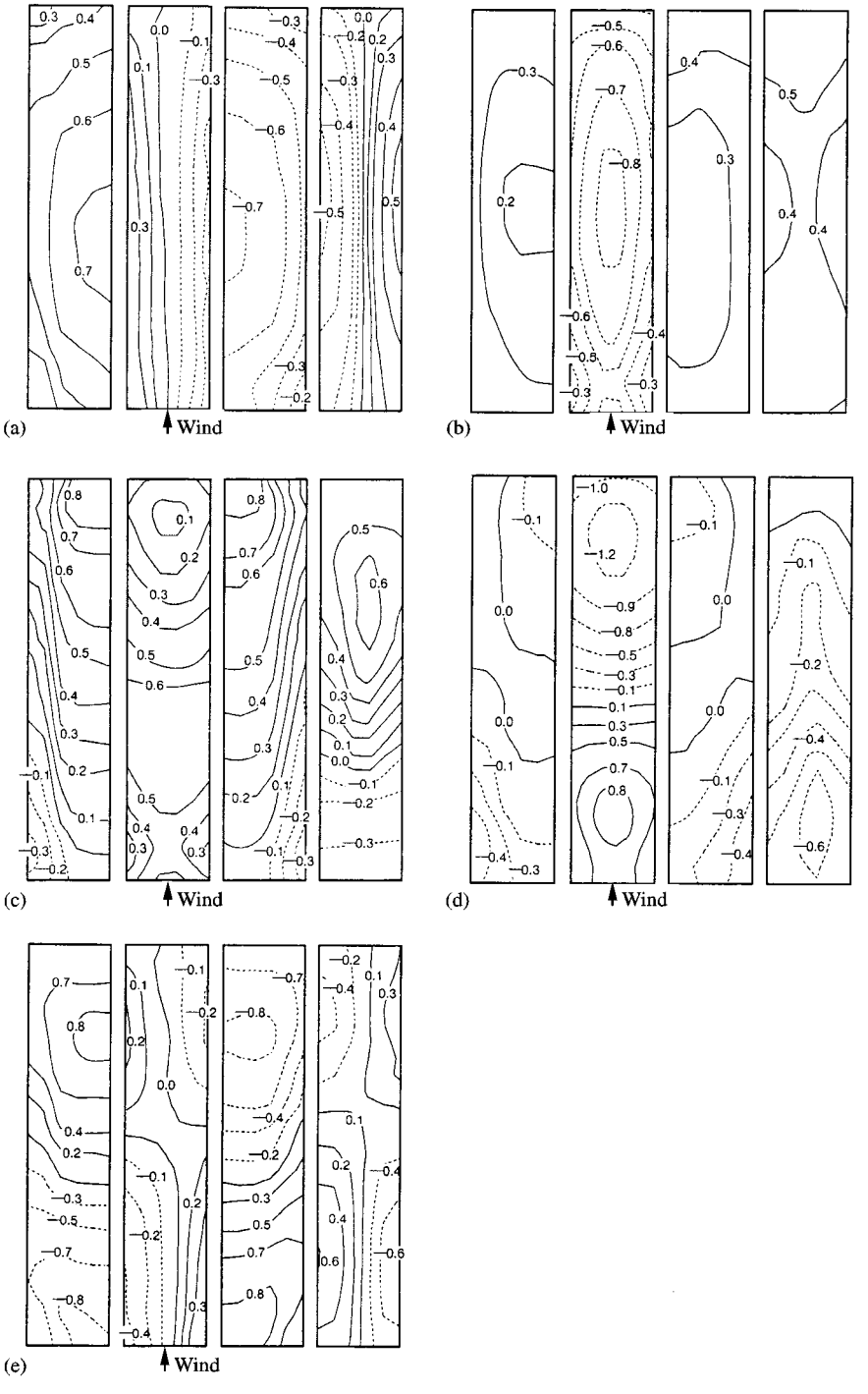

Figure 17. Eigenvectors (mode shapes) for the lowest five modes: (a) 1st mode; (b) 2nd mode; (c) 3rd mode; (d) 4th mode; (e) 5th mode.

across-wind force. The bilaterally antisymmetric pattern on the windward wall is similar to the horizontal gradient of the mean wind pressure field. Under the quasi-steady assumption, regarding the v-component of wind speed, the pressure field fluctuates in proportion to the mean pressure gradient with the flow angle for horizontal directions. Although the mean pressure gradient for the horizontal direction does not exactly equal that for the horizontal flow angle, the result suggests a quasi-steady relationship with the v-component of the fluctuating wind speed.

The 2nd mode shape is bilaterally symmetric, as shown in Figure 17(b). The 2nd mode becomes dominant for the along-wind force. The similarity between the mode shape and the mean wind pressure coefficient indicates a quasi-steady relationship with the u-component of the fluctuating wind speed, as discussed in an earlier section.

The 3rd mode shape is also bilaterally symmetric, as shown in Figure 17(c). This greatly contributes to the along-wind force. The large value near the top of the windward corner on the side wall suggests the effect of the highly three-dimensional flow near the top.

The 4th mode shape is similarly bilaterally symmetric, as shown in Figure 17(d). There is a large contribution to the along-wind force. The characteristic distribution on the windward wall is vertically nearly antisymmetric. Thus, when pushing the upper portion in the along-wind direction, it tends to pull the lower portion and it does not contribute to the along-wind base shear. However, it has a rotational effect on the building in the along-wind direction as a couple of forces. It is noted that this mode shape is similar to the vertical gradient of the mean wind pressure field on the windward wall. Under the quasi-steady assumption, regarding the w-component of wind speed, the pressure field fluctuates in proportion to the mean pressure gradient with the flow angle for the vertical direction. As with the v-component, the result also suggests a quasi-steady relationship with the w-component of the fluctuating wind speed.

The 5th mode shape is bilaterally antisymmetric as shown in Figure 17(e), similar to the 1st mode shape. It also greatly contributes to the across-wind force. The characteristic point of this mode shape is vertical antisymmetry. Therefore, there is very little contribution to base shear, but it contributes to the overturning effect in the across-wind direction.

3.3. Proportion of Each Mode

Table 4 shows the eigenvalue, proportion and cumulative proportion for each mode. The 1st mode contributes 26·3%, and the 2nd mode 16·7%. The cumulative proportion up to the 100th mode is 93·5%, while there are a total of 500 modes. This means that about 20% of the modes can reproduce a relatively detailed structure of the wind pressure fluctuations acting on each point of the building surface within an error ranging from 6 to 7%. It is necessary to match the detailed structures of the spatio-temporal fluctuation of the wind pressure for the localized wind pressure at individual points. However, for the wind forces given by their spatial integration, or for the response induced by them, the necessary number of modes can be further reduced as described later.

3.4. Power Spectral Density of the Principal Coordinate

Figure 18(a, b) shows the power spectral densities of the generalized wind forces and those of the lowest five principal coordinates. Linear vibration modes of the building were assumed for estimating the generalized wind forces. The power spectral density of the generalized across-wind force has a sharp peak of the Strouhal component due to Kármán vortex shedding, as shown in Figure 18(a). The power spectral densities of the 1st and the 5th principal coordinates also have a sharp peak at a similar position. It is found that the 1st

TABLE 4

Eigenvalues, proportions and cumulative proportions for the pressure field on a high-rise building model

Mode	Eigenvalue	Proportion (%)	Cumulative proportion (%)
1st	132·00	26·30	26·30
2nd	83·70	16·70	43·00
3rd	32·60	6·51	49·51
4th	25·80	5·16	54·67
5th	25·20	5·04	59·71
—	—	—	—
10th	7·19	1·44	71·43
—	—	—	—
50th	0·74	0·15	89·24
—	—	—	—
100th	0·26	0·05	93·47
—	—	—	—
300th	0·06	0·01	98·50
—	—	—	—
500th	0·01	0·00	100·00

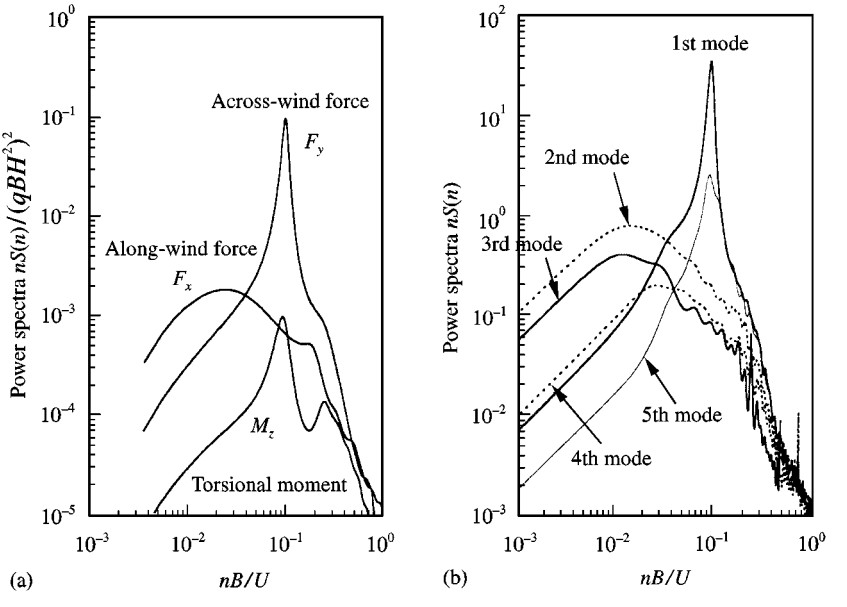

Figure 18. Power spectral densities: (a) generalized wind forces; (b) principal coordinates for the lowest five modes.

and 5th modes closely relate to the vortex shedding and greatly contribute to the across-wind force. However, the power spectral densities of the 2nd, the 3rd and the 4th principal coordinates do not have the Strouhal peak, but are similar to that of the generalized along-wind force. It is noted that the power spectral density of the generalized torsional moment has a Strouhal peak and a peak probably induced by re-attachment near the leeward edge of the side walls. It is supposed that mainly the 1st and the 5th modes may

relate to the torsional moment. This demonstrates that torque is mainly produced by the pressure distribution on the side walls due to vortex shedding, while the noncorrelation of pressure on the windward and leeward walls provides an almost negligible contribution, thus confirming previous observations in Isyumov & Poole (1984) and Solari (1985).

3.5. Vertical Distribution of Fluctuating Wind Force Coefficients and Contribution of Eigenmode

Figure 19(a–d) shows the vertical distributions of the fluctuating along-wind and across-wind force and torsional moment coefficients (standard deviation) obtained by each eigenvector and its principal coordinate, as well as those obtained from the original fluctuating wind pressure data.

As shown in Figure 19(a), the along-wind force coefficients depend mainly on the 2nd mode. The contributions of the 3rd and 4th modes are also large, but those of the others are negligible. The fluctuating wind force coefficient by the 4th mode increases in the upper and lower regions setting a node near the mid-height point. However, as shown in Figure 17(d), the 4th mode shape on the windward wall has opposite signs in the upper and lower parts. Therefore, the 4th mode along-wind wind forces in the upper and lower parts are mutually out of phase.

Figure 19(b) shows the fluctuating across-wind force coefficients. The greatest contribution comes from the 1st mode. The contribution of the 5th mode is also large, but those of the others are very low. The 5th mode fluctuating wind force coefficient also has a node near the mid-height point and there are high-value regions at the upper and lower parts. However, as shown in Figure 17(e), the 5th mode shape has opposite signs at the upper and lower parts of the side wall, and the 5th mode across-wind forces in the upper and lower parts are mutually out of phase.

As shown in Figure 19(c), the greatest contribution to the torsional moment comes from the 1st mode, and the 5th mode contribution is significant. The contributions of the relatively high-order mode are also large in the fluctuating torsional moment coefficient as shown in Figure 19(d) (Kikuchi *et al.* 1997).

3.6. Wind Force Determined from only a Few Dominant Modes

Figure 20(a–c) shows the temporal variations of generalized wind force coefficients reconstructed by only a few selected dominant modes.

The generalized along-wind force in Figure 20(a) was obtained from three modes, the 2nd, the 3rd and the 4th. That for across-wind in Figure 20(b) was obtained from only two modes, the 1st and the 2nd. The generalized torsional moment in Figure 20(c) was obtained from 10 selected dominant modes. For comparison, the original generalized fluctuating wind forces are also shown in the figures. The wind forces reconstructed by the selected two or three dominant modes almost completely coincide with the original generalized wind force coefficients. Considering that there are 500 modes in total, this is an amazing reduction in the amount of necessary information.

3.7. Results of Wind Response Analysis Using Wind Force Determined by only a Few Dominant Modes

Time-domain response analyses were conducted for the 25-lumped-mass system shown in Figure 14, where each mass has three degrees of freedom: along-wind, across-wind and torsion. The natural period of the fundamental vibration mode of the building was set at 5 s

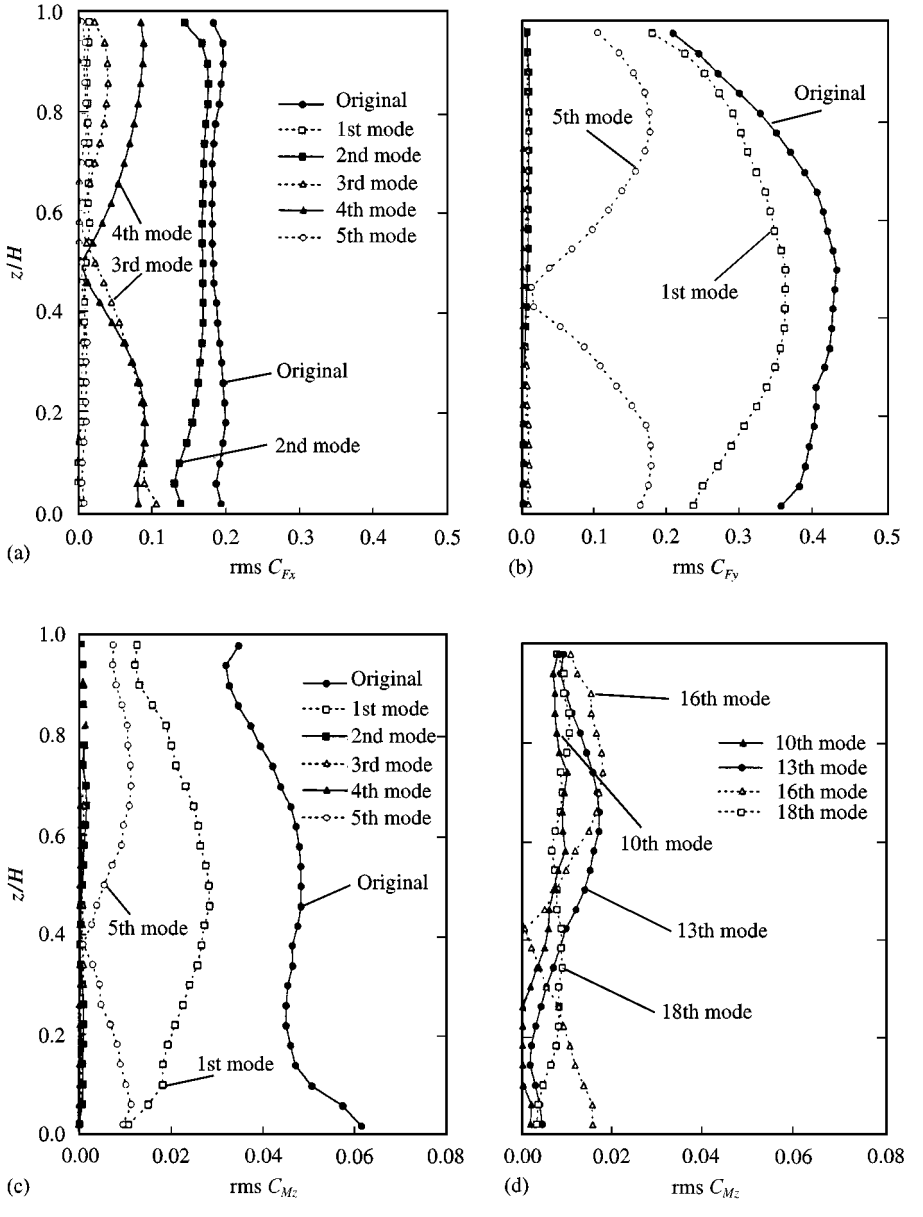

Figure 19. Vertical distribution of fluctuating wind force coefficients derived from each mode: (a) along-wind force; (b) across-wind force; (c) torsional moment; (d) torsional moment.

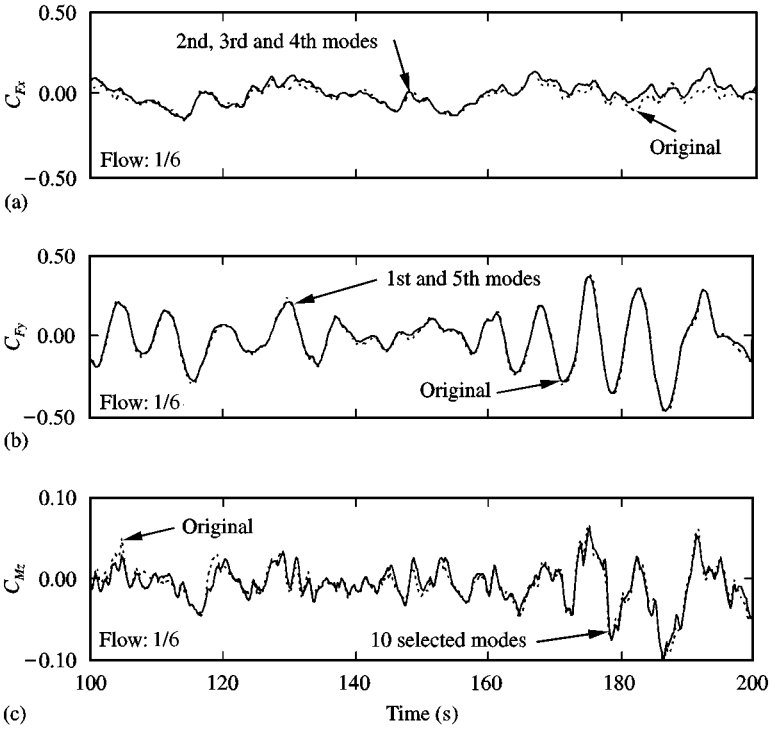

Figure 20. Temporal variations of generalized wind force coefficients reconstructed from the selected dominant modes: (a) along-wind force from the 2nd, 3rd, and 4th modes; (b) across-wind force from the 1st and 5th; (c) torsional moment from the 10 selected modes (1, 5, 10, 11, 13, 14, 16, 18, 21 and 31st modes).

for both translational directions, and at 3·8 s for torsion. The damping ratio to the critical value was set at 2% for the fundamental mode. The mean wind speed at the top ($H = 200$ m) was set at 55 m/s assuming a 100-year-recurrence wind speed in Tokyo. A response analysis was performed for 600 s with wind forces comprising the selected dominant modes according to the previous section: three modes for the along-wind force, and two modes for the across-wind force. Regarding the reconstructed torsional moment, 10 dominant modes were selected as described later in Table 5.

Figure 21(a–c) shows the temporal variations of the top responses. The results of the response analysis using the wind forces reconstructed by the selected dominant modes show very good agreement with the original responses. Figure 22(a–d) shows the vertical distributions of maximum values and standard deviations of displacement, shear force, overturning moment and torsional moment, respectively. Table 5 summarizes the maximum values, the standard deviations, and corresponding error rates for along-wind displacement, across-wind displacement and angular displacement at the top of the building. The responses using the wind forces reconstructed by only the selected dominant modes agree very well with the original responses, and the maximum error is less than 6%. It is thus demonstrated that POD can extract the essence of each wind force and can very efficiently reduce the necessary information for simulation.

5. CONCLUDING REMARKS

This paper has discussed the efficiency of POD and points to note in its application. However, the principal coordinate obtained by POD is still merely a coordinate. Even for

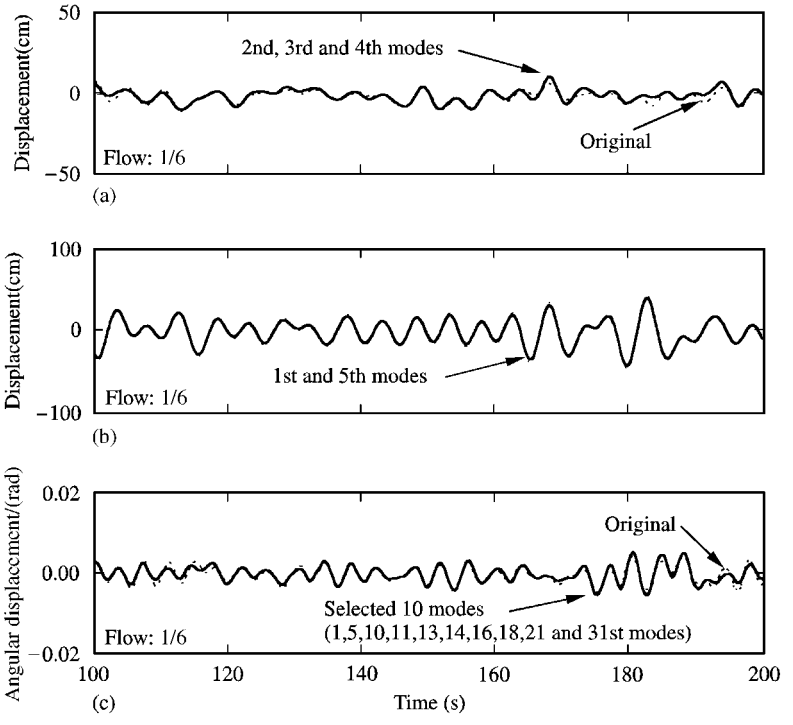

Figure 21. Temporal variations of the top responses analyzed using wind forces reconstructed by the selected dominant modes: (a) along-wind displacement; (b) across-wind displacement; (c) torsional angle.

TABLE 5

Results of response analyses using original wind forces and wind forces reconstructed from selected dominant modes

Wind forces	Response at the top ($H = 200$ m)					
	Along-wind displacement (cm)		Across-wind displacement (cm)		Angular displacement (rad)	
	max	s.d.	max	s.d.	max	s.d.
Original	21·3	6·67	56·6	16·8	0·0107	0·0025
Reconstructed from selected dominant modes*	22·5	6·46	53·7	15·9	0·0112	0·0026
Error (%)	5·6	3·1	5·1	5·7	4·8	3·4

* Along-wind force: 2nd, 3rd, and 4th modes.
Across-wind force: 1st and 5th modes.
Torsional moment: 1st, 5th, 10th, 11th, 13th, 14th, 16th, 18th, 21st and 31st modes.

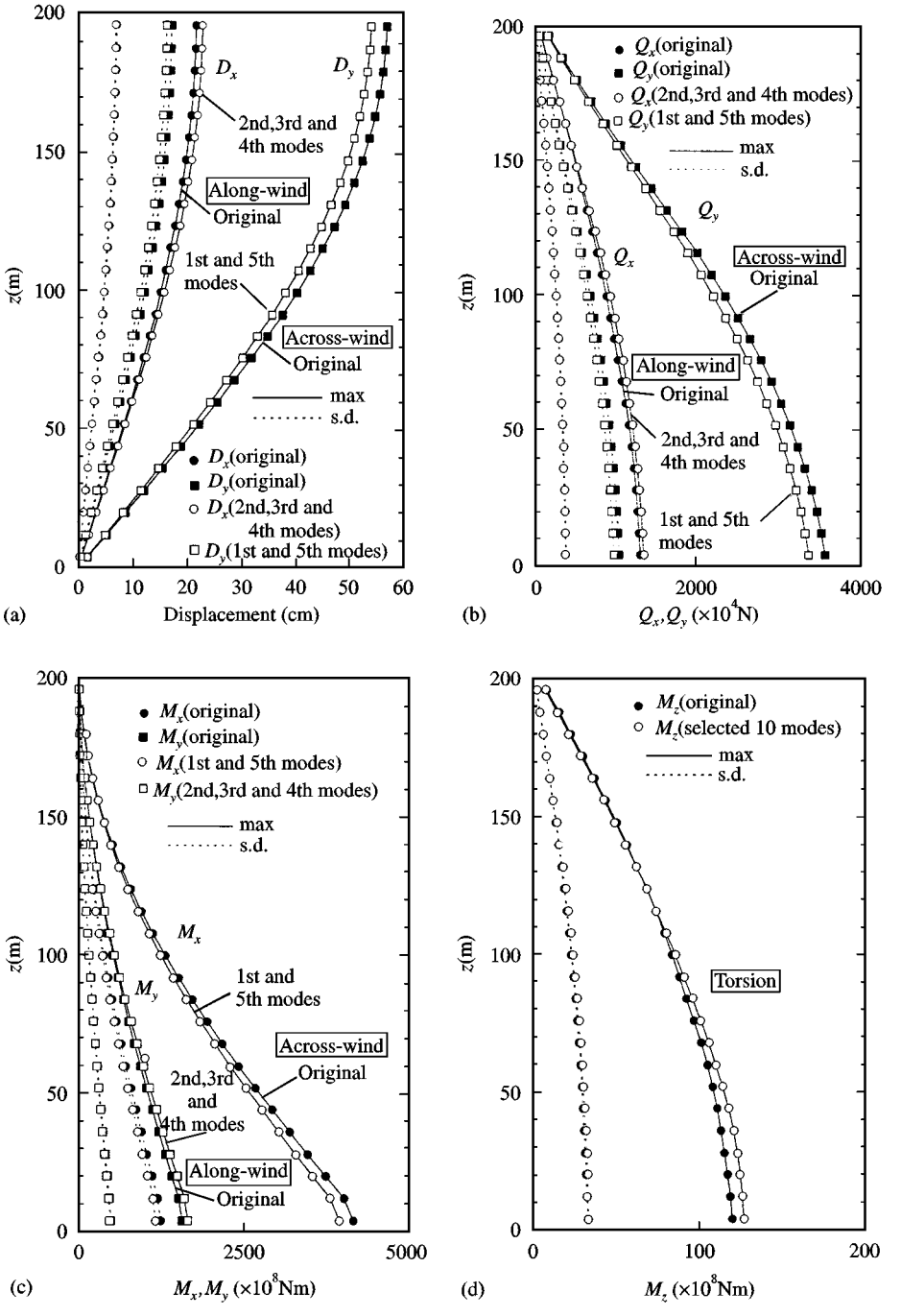

Figure 22. Vertical distribution of the maximum values and standard deviations due to response analysis using wind forces reconstructed by the selected dominant modes: (a) displacement; (b) shear force; (c) overturning moment; (d) torsional moment.

the first mode, its physical meaning is an interpretation of the result after it came out and cannot be generalized. Similarly, the other modes can also be compared with the various aspects of the results and some resultant interpretations can be efficiently made for the phenomena. As shown in the application examples presented in this paper, it is possible to relate the lower modes to physical phenomena such as vortex shedding, quasi-steady assumption, and so on. By relating to the physical phenomena to achieve another important purpose, it is possible to clarify the systematic structure hidden in the random fluctuation. This work in determining the relationship itself can enhance understanding of the phenomena and the research itself. Another practical effect of POD is a significant reduction in amount of information that needs be collected.

The authors emphasize that the mean value components have to be excluded in the spatial correlation matrix, so that it should strictly be the covariance matrix. The eigenvectors obtained with inclusion of the mean value components are contaminated by the mean value vector, and have no physical relation with the characteristics of fluctuation of the random field.

As POD is a method for extracting the hidden systematic structure from random information, it can be thought of as a kind of filtering technique. It can also be applied to cases where it is necessary to remove the noise from noisy data in field measurements of vibration modes and so on.

ACKNOWLEDGEMENTS

The authors would like to acknowledge discussions with Prof. B. Bienkiewicz of Colorado State University.

References

Armitt, J. 1968 Eigenvector analysis of pressure fluctuations on the West Burton instrumented cooling tower. Central Electricity Research Laboratories (U.K.) Internal Report RD/L/N 114/68.

Best, R. J. & Holmes, J. D. 1983 Use of eigenvalues in the covariance integration method for determination of wind load effects. *Journal of Wind Engineering and Industrial Aerodynamics* **13,** 359–370.

Bienkiewicz, B. & Ham, H. J. 1993 Proper orthogonal decomposition of roof pressure. *Journal of Wind Engineering and Industrial Aerodynamics* **50,** 193–202.

Bienkiewicz, B., Tamura, Y., Ham, H. J., Ueda, H. & Hibi, K. 1995 Proper orthogonal decomposition and reconstruction of multi-channel roof pressure. *Journal of Wind Engineering and Industrial Aerodynamics* **54–55,** 369–381.

Davenport, A. G. 1995 How can we simplify and generalize wind loads? *Journal of Wind Engineering and Industrial Aerodynamics* **54–55,** 657–669.

Fujii, K., Hibi, K. & Ueda, H. 1986 A new measuring system using electrically scanned pressure sensors (ESP) and some applications of the ESP system to a square building shape. In *Proceedings of the 9th National Symposium on Wind Engineering*, Tokyo, Japan, December 1986, pp. 313–318.

Holmes, J. D. 1990 Analysis and synthesis of pressure fluctuations on bluff bodies using eigenvectors. *Journal of Wind Engineering and Industrial Aerodynamics* **33,** 219–230.

Holmes, J. D. 1992 Optimised peak load distributions. *Journal of Wind Engineering and Industrial Aerodynamics* **41–44,** 267–276.

Holmes, J. D., Denoon, R., Kwok, K. C. S. & Glanville, M. J. 1997 Wind loading and response of large stadium roofs. In *Proceedings of the IASS International Symposium on Shell and Spatial Structures*, *Singapore*, 10–14 November 1997, pp. 317–324.

Holmes, P., Lumley, J. L. & Berkooz, G. 1996 *Turbulence*, *Coherent Structures*, *Dynamical Systems and Symmetry*. Cambridge: Cambridge University Press.

Isyumov, N. & Poole, M. 1984 Wind induced torque on square and rectangular building shapes. *Journal of Wind Engineering and Industrial Aerodynamics* **13,** 183–196.

KAREEM, A. & CERMAK, J. E. 1984 Pressure fluctuations on a square building model in boundary-layer flows. *Journal of Wind Engineering and Industrial Aerodynamics* **16,** 17–41.

KIKUCHI, H., TAMURA, Y., UEDA, H. & HIBI, K. 1997 Dynamic wind pressures acting on a tall building model — proper orthogonal decomposition. *Journal of Wind Engineering and Industrial Aerodynamics* **69–71,** 631–646.

LEE, B. E. 1975 The effects of turbulence on the surface pressure field of a square prism. *Journal of Fluid Mechanics*, **69,** 263–282.

SANTI, F. & HÉMON, P. 1998 Wake analysis of a H-section cylinder versus wind tunnel blockage. Presented at *The 2nd East European Conference on Wind Engineering*, Prague, Czech Republic, 7–11 September 1998.

SOLARI, G. 1985 Mathematical model to predict 3-D wind loading on buildings. *Journal of Engineering Mechanics* **111,** 2, 254–276.

TAMURA, Y. 1995 An introduction of applying proper orthogonal decomposition to random fields, *Journal of Wind Engineering*, *Transactions of the Japan Association for Wind Engineering*, **65,** 33–41 (in Japanese).

TAMURA, Y., UEDA, H., KIKUCHI, H., HIBI, K., SUGANUMA, S. & BIENKIEWICZ, B. 1995 Proper orthogonal decomposition study of approach wind-building pressure correlation. In *Proceedings of the Ninth International Conference on Wind Engineering*, *Retrospect and Prospect*, Vol. IV, pp. 2115–2126.

UEDA, H., HIBI, K., TAMURA, Y. & FUJII, K. 1994 Multi-channel simultaneous fluctuating pressure measurement system and its application. *Journal of Wind Engineering and Industrial Aerodynamics* **51,** 1, 93–104.